

# Multimodal matching using a Hybrid Convolutional Neural Network

Elad Ben Baruch  
Ben-Gurion University of the Negev  
eladbenb@post.bgu.ac.il

Yosi Keller  
Bar Ilan University  
Yosi.keller@gmail.com

## Abstract

In this work we propose a novel Convolutional Neural Network (CNN) architecture for the matching of pairs of image patches acquired by different sensors. Our approach utilizes two CNN sub-networks, where the first is a Siamese CNN and the second is a subnetwork consisting of dual non-weight-sharing CNNs. This allows simultaneous joint and disjoint processing of the input pair of multimodal image patches. The convergence of the training and the test accuracy is improved by introducing auxiliary losses, and a corresponding hard negative mining scheme. The proposed approach is experimentally shown to compare favorably with contemporary state-of-the-art schemes when applied to multiple datasets of multimodal images. The code implementing the proposed scheme was made publicly available.

## 1 Introduction

The matching of feature points in images is a fundamental task in computer vision and image processing, that is applied in common computer vision applications such as image registration [29], dense image matching, [24], and 3D reconstruction [1], to name a few. The term *feature point* relates to the center of an image patch, where a feature point is expected to be salient and to be identified in multiple images of the same scene, that might differ by pose and lighting conditions [18]. A *detector* identifies the location of a feature points, and the surrounding patch is encoded by a *descriptor*.

The matching of feature points in images acquired by different image modalities, as depicted in Fig. 1, is of

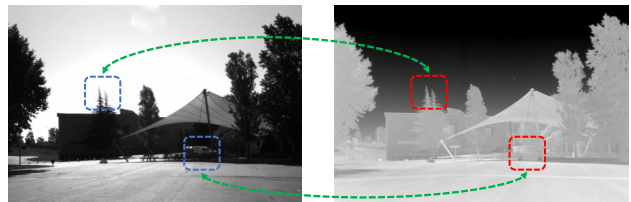


Figure 1: The multisensor patch matching problem. The matched optical (left) and IR (right) images differ by significant appearance changes due to the different physical characteristics captured by the different sensors. The images are part of the LWIR-RGB dataset [2].

particular interest in remote sensing [14, 17, 15, 12] and medical imaging [21], as the fusion of multi-spectral images provides information synergy. The acquisition of the same scenes by different sensors might result in significant appearance variations, that might be nonlinear and unknown apriori, such as non-monotonic intensity mappings, contrast reversal, and non-corresponding edges and textures.

Given multimodal input images  $\mathbf{I}_1$  and  $\mathbf{I}_2$ , their registration can be formulated as the direct estimation of a parametric global transformation  $T$ , such as rigid, and affine transformations, by minimizing an appearance invariant similarity measures  $\phi(\mathbf{I}_1, \mathbf{I}_2)$ , such as mutual information [26], with respect to the global geometric transformation  $T$

$$T^* = \arg \min_T \phi(\mathbf{I}_1, T(\mathbf{I}_2)), \quad (1)$$

where  $T(\mathbf{I}_2)$  is the image  $\mathbf{I}_2$  warped to  $\mathbf{I}_1$  based on  $T$ . Gradient-based approaches were applied by Irani et al.

[14], and Keller et al. [15] to appearance-invariant image representations to solve Eq. 1 iteratively.

Other multimodal registration schemes are based on matching *local* image features such as patches, contours [17] and corners. Such approaches match the set of interest points  $S_1 \in \mathbf{I}_1$  to the set  $S_2 \in \mathbf{I}_2$ , where each feature points  $s_i \in S_i$  is first detected, and then encoded by a robust appearance-invariant representation, denoted as a *descriptor*, such that  $D(s)$  is the descriptor of the point  $s$ , and a pair of descriptors can be matched by computing their  $L_2$  distance

$$d(s_1, s_2) = \|D(s_1) - D(s_2)\|_2. \quad (2)$$

Such descriptors were commonly derived by extending unimodal descriptors such as SIFT and Daisy [18, 23] to the multimodal case [8, 13, 2, 3, 16].

Convolutional Neural Networks (CNNs) were applied to feature point matching [20, 4], by learning to compute data-driven multimodal image descriptors.

These CNNs are trained by optimizing a metric such as the Hinge Loss, while others [28, 5, 10] aim to compute a similarity score between image patches by optimizing a Softmax loss by classifying each pair of patches as same/not-same. Such approaches utilize Siamese CNNs [4] consisting of weight sharing sub-networks.

The upside of  $L_2$ -based representations compared to those computed using the Softmax loss, is their reduced computational complexity when applied to matching sets of feature points detected in a pair or set of images.  $K$  nearest neighbors (KNN) similarity search via  $L_2$ -based representations can be computationally accelerated using metric embedding schemes such as LSH [11] and Min-Hash [6].

In this work we propose a CNN-based metric learning approach for unimodal feature points matching, that estimates the similarity of pairs of image patches acquired by different sensors. In particular, we extend the Siamese architecture and present the Hybrid CNN architecture consisting of both a Siamese sub-network and a dual-channel non-weight-sharing *asymmetric* sub-network. The use of the asymmetric sub-network is due to the inherent asymmetry in the multisensor matching problem, where the heterogeneous inputs might differ significantly, and thus require different processing implemented by the *asymmetric* sub-network. In particular, each branch of the asym-

metric sub-network estimates a *modality-specific* adaptive representation of the multisensor patches.

Thus, we aim to leverage both the joint and disjoint information in the multimodal images, using the Siamese and Asymmetric subnets, respectively. Siamese sub-networks were previously shown [4] to yield accurate matching results, and are outperformed by the proposed Hybrid scheme. The Siamese and Asymmetric subnets are optimized by corresponding auxiliary losses, and their outputs are merged and optimized to yield the final results. We derive a corresponding hard mining scheme to improve the classification accuracy and training convergence.

In particular, we propose the following contributions:

**First**, we propose a novel hybrid CNN architecture consisting of both a Siamese and asymmetric sub-networks, able to leverage both the joint and disjoint information in multimodal patches, to determine their similarity.

**Second**, we show that the use of auxiliary losses in hybrid architectures improves the convergence of each sub-network during training, and the convergence of the hybrid model.

**Third**, we propose an effective and computationally efficient hard negative mining scheme that is shown to significantly improve the matching accuracy.

**Last**, the proposed scheme was experimentally shown to compare favorably with contemporary schemes when applied to state-of-the-art multimodal image matching benchmarks [4, 10] and the corresponding source-code was made available publicly<sup>1</sup>.

## 2 Related work

Common approaches for computing appearance-invariant image representations of multisensor images, utilize image edges and contours that are salient in multimodal images. Irani et al. [14] suggested a coarse-to-fine scheme for estimating the global parametric motion (affine, rigid) between multimodal images, using the magnitudes of directional derivatives as a robust image representation. The correlation between these representations is maximized using iterative gradient methods, and a coarse-to-fine formulation.

<sup>1</sup><https://github.com/eladbb/HybridSiamese>

Keller et al. [15] proposed the “Implicit Similarity” formulation that is an iterative scheme utilizing gradient information for global alignment. A set of pixels with maximal gradient magnitude is detected in one of the input images, rather than contours and edges as in [14]. The gradient of the corresponding points in the second image is maximized with respect to a global parametric motion, without explicitly maximizing a similarity measure.

The seminal work of Viola and Wells [26] on applying the mutual information (MI) similarity to multisensor image matching, utilized a statistical representation of the images, while optimizing their mutual information with respect to the motion parameters. Due to the nonlinearity of the MI functional, its optimization entails numerical difficulties.

Modality-invariant descriptors were often designed by modifying the seminal SIFT [18] descriptor [8]. Contrast-invariance was achieved by mapping the gradient orientations of the interest points from  $[0, 2\pi)$  to  $[0, \pi)$  by mirroring and averaging. Hasan et al. showed that such descriptors reduce the matching accuracy [13], and further modified the SIFT descriptor [12] by thresholding gradient values to reduce the effect of strong edges. An enlarged spatial window with additional sub-windows was used to improve the spatial resolution.

Aguilera et al. [2] used a histogram of contours and edges instead of a gradients histogram to avoid the ambiguity of the SIFT descriptor when applied to multimodal images, while the dominant orientation was determined similarly. This approach was improved by the same authors by applying multi-oriented and multi-scale Log-Gabor filters [3]. The Duality Descriptor (DUDE) multimodal descriptor was proposed by Kwon et al. [16], where each line segment near a keypoint is encoded by a 3D histogram of radial, angular and length parameters. This approach encodes the geometry of the line segment and is invariant to appearance variations.

With the emergence of CNNs as the state-of-the-art approach to a gamut of computer vision problems, such approaches were applied to patch matching. Zagoruyko and Komodakis [28] proposed several CNN architectures for matching single modality patches, such as a Siamese CNN with an  $L_2$  or a Softmax loss, and a CNN where the input patches are stacked as different image channels, and the stacked image is classified by the CNN. Aguilera et al. [4] applied Zagoruyko and Komodakis’ approaches

[28] to matching multimodal patches and showed that the resulting CNN outperformed the state-of-the-art multimodal descriptors. The stacked CNN architecture proved to be the most accurate.

To alleviate the significant computational complexity of the stacked approach when applied to sets of feature points, Aguilera et al. proposed the Q-Net CNN [5] that was trained using an  $L_2$  loss. The Q-Net CNN consists of four weight sharing sub-networks and two corresponding pairs of input patches, that allow hard negative mining. This approach was shown to achieve state-of-the-art accuracy when applied to the Vis-Nir benchmark [4] using  $L_2$  matching.

Recent work by En et al. [10] introduced a hybrid Siamese CNN, similar to the proposed scheme, denoted as TS-Net, for multimodal patch matching, consisting of Siamese and asymmetric sub-networks, utilizing a Softmax loss on top. Compared to the proposed scheme, this approach does not compute  $L_2$ -optimized patch encodings that are essential for the matching of images, that typically consist of multiple ( $O(100)$ ) patches per image, as discussed in Section 3.1. Each of the sub-networks outputs a scalar Softmax output that is merged using an FC layer of dimension four. Our proposed scheme is experimentally shown in Section 4 to compare favorably with the TS-Net [10] results.

### 3 Multimodal image matching using Hybrid metric learning

In this section, we present the proposed hybrid multisensor matching scheme depicted in Fig. 2. Let  $\mathbf{x}_i \in \mathbf{I}_1$  and  $\mathbf{y}_i \in \mathbf{I}_2$  be a pair of multi-dimensional image patches acquired by different modalities. We aim to compute a corresponding representation,  $\hat{\mathbf{x}}_i$  and  $\hat{\mathbf{y}}_i$ , respectively. The descriptors are optimized with respect to two objectives. The first is the Hinge Loss applied to the  $L_2$  distance, while the second, infers a binary classification using a Softmax loss.

The Hybrid network learns both the joint and disjoint characteristics of multisensor patches, using a Siamese and asymmetric (non-weight-sharing) sub-networks. The Siamese sub-network learns a single mapping for both input modalities, denoted as  $W_s(\mathbf{x}_i)$  and  $W_s(\mathbf{y}_i)$ , respec-

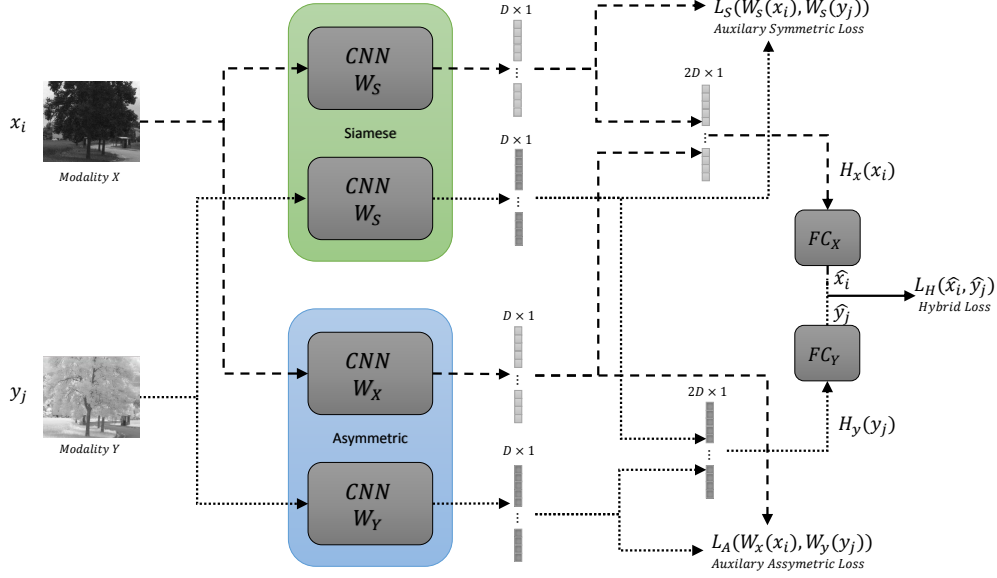


Figure 2: The proposed hybrid matching model, consisting of two sub-networks: a Siamese sub-network and an asymmetric sub-network with non-shared weights.

tively, in Fig. 2, while the asymmetric sub-network estimates a different, modality-specific mapping for each modality,  $W_x(\mathbf{x}_i)$  and  $W_y(\mathbf{y}_i)$ , respectively. The outputs of the sub-networks are concatenated, such that

$$\begin{aligned} H_x(\mathbf{x}_i) &= [W_s(\mathbf{x}_i), W_x(\mathbf{x}_i)]^T, \\ H_y(\mathbf{y}_i) &= [W_s(\mathbf{y}_i), W_y(\mathbf{y}_i)]^T, \end{aligned} \quad (3)$$

and the FC layers  $FC_S$  and  $FC_A$  are applied to  $H_x(\mathbf{x}_i)$  and  $H_y(\mathbf{y}_i)$ , respectively. Such that

$$\begin{aligned} \hat{\mathbf{x}}_i &= FC_x(H_x(\mathbf{x}_i)), \\ \hat{\mathbf{y}}_i &= FC_y(H_y(\mathbf{y}_i)) \end{aligned} \quad (4)$$

are the Hybrid encodings  $\hat{\mathbf{x}}_i$  and  $\hat{\mathbf{y}}_i$  of the inputs  $\mathbf{x}_i$  and  $\mathbf{y}_i$ , respectively.  $\hat{\mathbf{x}}_i$  and  $\hat{\mathbf{y}}_i$  are computed by optimizing the hybrid loss  $L_H(\hat{\mathbf{x}}_i, \hat{\mathbf{y}}_i)$ , being either a Softmax or  $L_2$  losses.

The choice of the loss relates to the task of the overall network. The Softmax estimates the matching probability, while the  $L_2$  loss yields a descriptor-based representation of the matched images, that can be utilized in large-scale patch retrieval schemes, as a  $K$  nearest neighbors (KNN)

$L_2$  search can be computationally accelerated by applying approximate KNN schemes such as LSH [11] and Min-Hash [6].

To improve the convergence of the proposed scheme, the auxiliary losses  $L_s(W_s(\mathbf{x}_i), W_s(\mathbf{y}_i))$  and  $L_A(W_x(\mathbf{x}_i), W_y(\mathbf{y}_i))$ , are applied to the outputs of the Siamese and asymmetric sub-networks, respectively. These losses are the same as the one used in the main Hybrid loss.

### 3.1 Computationally efficient multimodal matching

The proposed scheme allows matching a pair of patches  $\mathbf{x}_i \in \mathbf{X}$  and  $\mathbf{y}_i \in \mathbf{Y}$ . Yet, in common image matching problems one aims to match sets of points  $\{\mathbf{x}_i\} \in \mathbf{X}$  and  $\{\mathbf{y}_j\} \in \mathbf{Y}$ , such that for each point  $\mathbf{x}_i \in \mathbf{X}$  we aim to find the  $K \geq 1$  points  $\{\mathbf{y}_j\} \in \mathbf{Y}$  that are the nearest to  $\mathbf{x}_i$  regarding the  $L_2$  norm or (Softmax-based) matching probability.

The use of the proposed scheme allows computing  $\hat{\mathbf{x}}_i$  and  $\hat{\mathbf{y}}_i$ , the descriptors encoding the images  $\mathbf{x}_i$  and  $\mathbf{y}_i$ ,

separately. In particular, the encodings of separate batches of the input images  $\{\mathbf{x}_i\}$  and  $\{\mathbf{y}_i\}$  can be efficiently computed. Thus, given the encodings  $\{\hat{\mathbf{x}}_i\}$  and  $\{\hat{\mathbf{y}}_i\}$  a fast  $L_2$  KNN search can be applied [11, 6].

The estimation of the Softmax measure between a pair of samples  $\mathbf{x}_i$  and  $\mathbf{y}_i$  requires to apply the Softmax function to  $\hat{\mathbf{x}}_i + \hat{\mathbf{y}}_i$ . The following derivation shows that applying an FC layer to the concatenation  $[H_x(\mathbf{x}_i) \ H_y(\mathbf{y}_i)]^T$  is equivalent to summing the encodings.

$$\begin{aligned} \text{FC} \begin{bmatrix} H_x(\mathbf{x}_i) \\ H_y(\mathbf{y}_i) \end{bmatrix} &= [\text{FC}_x \ \text{FC}_y] \begin{bmatrix} H_x(\mathbf{x}_i) \\ H_y(\mathbf{y}_i) \end{bmatrix} \\ &= [\text{FC}_x \ \mathbf{0}] \begin{bmatrix} H_x(\mathbf{x}_i) \\ H_y(\mathbf{y}_i) \end{bmatrix} + [\mathbf{0} \ \text{FC}_y] \begin{bmatrix} H_x(\mathbf{x}_i) \\ H_y(\mathbf{y}_i) \end{bmatrix} \\ &= \text{FC}_x \cdot H_x(\mathbf{x}_i) + \text{FC}_y \cdot H_y(\mathbf{y}_i) = \hat{\mathbf{x}}_i + \hat{\mathbf{y}}_i \end{aligned}$$

### 3.2 Hybrid CNN architecture

For both  $L_2$  and Softmax losses, the same architecture was used for both Siamese and asymmetric sub-network. The CNN for the  $L_2$  loss is detailed in Table 1, consisting of five convolution layers followed by RELU activations, as well as two pooling layers after the first three convolution layers. We use an FC layer at the end of each branch alongside unit norm normalization.

Layer	Output	Kernel	Stride	Pad
Conv0	$64 \times 64 \times 32$	$5 \times 5$	1	2
Pooling	$32 \times 32 \times 32$	$3 \times 3$	2	-
Conv1	$32 \times 32 \times 64$	$5 \times 5$	1	2
Pooling	$16 \times 16 \times 64$	$3 \times 3$	2	-
Conv2	$16 \times 16 \times 128$	$3 \times 3$	1	1
Pooling	$8 \times 8 \times 128$	$3 \times 3$	2	-
Conv3	$6 \times 6 \times 256$	$3 \times 3$	1	0
Conv4	$4 \times 4 \times 256$	$3 \times 3$	1	0
FC	$1 \times 128$	-	-	-
Unit norm	$1 \times 128$	-	-	-

Table 1: The CNN architecture of the sub-networks using the  $L_2$  Hinge loss. Each sub-network accepts a  $64 \times 64$  patch and outputs a  $128 \times 1$  descriptor.

The output of each sub-network is optimized by the auxiliary losses,  $L_S$  and  $L_A$ , where a Hinge loss was ap-

plied to the  $L_2$  distance

$$L(\mathbf{x}_i, \mathbf{y}_i) = \begin{cases} \|D(\mathbf{x}_i) - D(\mathbf{y}_i)\|_2; & \mathbf{x}_i = \mathbf{y}_i \\ \max(0, C - \|D(\mathbf{x}_i) - D(\mathbf{y}_i)\|_2); & \mathbf{x}_i \neq \mathbf{y}_i \end{cases} \quad (5)$$

and we set  $C = 1$ . A similar CNN architecture, detailed in Table 2, was applied for the Softmax loss CNN.

Layer	Output	Kernel	Stride	Pad
Conv0	$64 \times 64 \times 32$	$5 \times 5$	1	2
Pooling	$32 \times 32 \times 32$	$3 \times 3$	2	-
Conv1	$32 \times 32 \times 64$	$5 \times 5$	1	2
Pooling	$16 \times 16 \times 64$	$3 \times 3$	2	-
Conv2	$16 \times 16 \times 128$	$3 \times 3$	1	1
Pooling	$8 \times 8 \times 128$	$3 \times 3$	2	-
Conv3	$6 \times 6 \times 256$	$3 \times 3$	1	0
Conv4	$4 \times 4 \times 256$	$3 \times 3$	1	0
Conv5	$2 \times 2 \times 256$	$3 \times 3$	1	0
FC	$1 \times 128$	-	-	-

Table 2: The CNN architecture of the sub-networks using the Softmax loss. Each sub-network accepts a  $64 \times 64$  patch and outputs a  $128 \times 1$  descriptor.

### 3.3 Hard negative mining

In patch matching the number of negative training samples is significantly larger than that of positive ones, and the common approach of generating negative training samples by randomly pairing non-matching patches [22, 5, 20], might lead to ‘easy’, non-informative negative pairs with large negative classification margins  $m$ . Such margins  $m > C$  will result in zero gradients in the  $L_2$  Hinge Loss as in Eq. 5, and in the saturation range of the Softmax loss, as depicted in Fig. 3.

To harness the relatively small fraction of informative negative patches, we propose a hard negative mining scheme [22, 20, 9] adapted to the patch matching problem. As the training set consists of pairs of patches, where each patch is acquired by a different sensor, for each set of  $N$  positive pairs, one can utilize  $N - 1$  negative pairs. Computing all  $N(N - 1)$  similarity scores (using  $L_2$  or Softmax) directly to find the hardest negatives might prove computationally exhaustive.



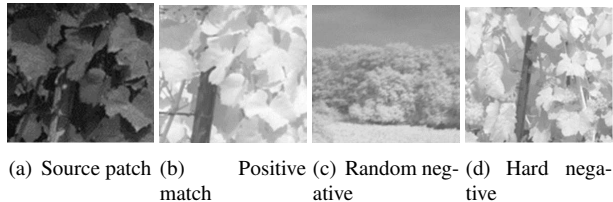


Figure 3: The matching of positive and negative pairs of multimodal image patches.

Hence, we utilize the proposed CNN to compute descriptors, such that given  $N$  pairs of patches, we compute the corresponding  $2N$  encodings  $\{\hat{\mathbf{x}}_i\}$  and  $\{\hat{\mathbf{y}}_i\}$ , choose  $M$  random patches from  $\{\hat{\mathbf{x}}_i\}$ , and search in  $\{\hat{\mathbf{y}}_i\}$  for the corresponding hardest negative samples. The remaining  $N - M$  negative pairs are randomly drawn. This hard mining approach is experimentally shown in Section 4 to improve the matching accuracy significantly.

## 4 Experimental Results

The proposed Hybrid scheme was experimentally verified by applying it to multi-spectral image datasets and benchmarks used in contemporary state-of-the-art schemes. The first was suggested by Aguilera et al. [4] consisting of a set of matching and non-matching pairs of patches, extracted from nine categories of the public VIS-NIR scene dataset [7]. The feature points were detected by an interest point detector and matched manually. The generated dataset as well as some of the images from the dataset are depicted in Fig. 4.

We also used the Vehicle Detection in Aerial Imagery (VEDAI) [19] dataset of multispectral aerial images, and the CUHK [27] dataset consisting of 188 faces and corresponding artist drawn sketches. These multimodal datasets are spatially pre-aligned, same as the VIS-NIR dataset, and were used by En et al. [10] to create an annotated training and test sets by extracting corresponding pairs of patches on a lattice grid. We evaluated the proposed scheme using the experimental setups and datasets used by Aguilera et al. [4, 5] and En et al. [10] and the results are detailed in Sections 4.3 and 4.4, respectively. The Hybrid was trained using stochastic gradient descent with a momentum of 0.9 and batch size of 128, learning

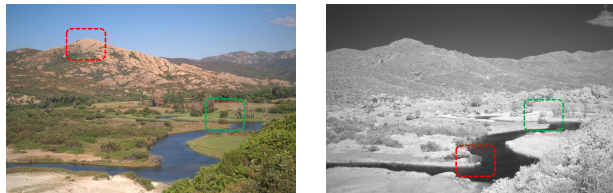


Figure 4: Positive and negative pairs of multimodal images patches extracted from the VIS-NIR dataset [4]. The positive pair is marked in green, while the negative one is marked in red.

rate of 0.01 and weight decay of 0.0005, where the same hyperparameters were used for training both  $L_2$  and Softmax losses. The learning rate was reduced by a factor of 0.1 after 75 epochs and again after 20 additional epochs. Early stoppage was applied to avoid overfitting where no loss reduction was archived in ten training iterations.

The networks parameters were initialized by a normal distribution, where the asymmetric subnets were initialized identically to improve convergence. In particular, this proved useful while training using the  $L_2$  loss.

In both setups, patches of 64x64 pixels were extracted and augmented by horizontal and vertical flipping, and the patches of each modality were normalized separately by subtracting their mean, and dividing by their standard deviation. The hard negative mining, detailed in Section 3, was applied using  $h_m = 0.8$ , and we study the optimal choice of  $h_m$  in Section 4.2. The matching accuracy is quantified by the false positive rate at 95% recall (FPR95), same as in [4, 5].

The Hybrid CNN was implemented using the MatConvNet [25] deep learning framework, where we trained both configurations using a single NVIDIA TitanX GPU. The source-code of the proposed scheme was made available publicly<sup>2</sup>.

The applicability of the auxiliary loss and hard negative mining is studied in Sections 4.1 and 4.2, respectively. We compare the results of the proposed Hybrid scheme using both  $L_2$  and Softmax losses to contemporary state-of-the-art approaches in Sections 4.3 and 4.4.

<sup>2</sup><https://github.com/eladbb/HybridSiamese>

## 4.1 Auxiliary losses

The auxiliary losses, detailed in Section 3, were added on top of each of the sub-networks of the Hybrid model, such that when the main loss is an  $L_2$  hinge loss, both auxiliary losses are  $L_2$  hinge losses. The same mutatis mutandis applies when using a Softmax loss. To evaluate their effectivity, we trained multiple configurations of the patch matching CNN, consisting of Siamese, asymmetric and Hybrid CNNs, where the hybrid CNN is applied with/without auxiliary losses and report the training and validation loss at the network output in Fig. 5. It follows that the Hybrid CNN outperforms the Siamese and asymmetric CNNs in terms of the loss, and that using the auxiliary losses allows to further reduce both the training and validation losses for both  $L_2$  and Softmax losses.

## 4.2 Hard negative mining

As most negative training examples chosen randomly might become non-informative after a few training epochs, we proposed in Section 3.3 to apply a hard negative mining scheme, where at each iteration, given  $N$  positive pairs we find the  $h_m N$ ,  $h_m \in [0, 1]$  negative pairs having the largest similarity probability, or minimal  $L_2$  distance for the Softmax and  $L_2$  losses, respectively. As  $h_m \rightarrow 1$  the number of negative pairs increases as well as the computational complexity required for their computation. The effectivity of this approach is exemplified in Fig. 6 where we depict the validation classification accuracy of the VIS-NIR benchmark test set in terms of the FPR95, using the proposed Hybrid scheme.

## 4.3 VIS-NIR benchmark results

The proposed Hybrid scheme was experimentally evaluated using the VIS-NIR dataset [4], and was compared to the state-of-the-art results of Aguilera et al. [4, 5] and En et al. [10] using the same experimental setup. As Aguilera et al. [4, 5] report on this dataset and experimental setup, we quote their results, while we evaluated the approach of En et al. [10] by training their publicly available code <sup>3</sup>.

All of the schemes were trained using the 'Country' category, where we utilized 80% of the given training

pairs of patches for training the Hybrid scheme using the Softmax loss, and  $L_2$  Hinge loss.

The results are reported in Table 3, where it follows that the proposed Hybrid scheme compares favorably with the previous schemes in terms of the mean error of 2.77 compared to a mean error of 4.47 of the previously leading scheme [4]. It also outperforms the previous schemes in all but two image categories.

## 4.4 En et al. [10] benchmark results

We also evaluated the proposed scheme using the experimental setup proposed by En et al. [10] where the VEDAI [19], CUHK [27] and VIS-NIR [4] datasets were sampled on a uniform lattice grid, and the results are reported in Table 4.

We quote the results reported by En et al. [10] on these datasets and setup, and trained the publicly available code<sup>4</sup> of Aguilera et al. [4, 5] and the proposed Hybrid scheme, using 70% of the data in each dataset for training, 10% for validation and 20% for testing. We also applied the modality-invariant descriptors [3] of Aguilera et al. using their publicly available code<sup>5</sup> and the SIFT descriptor [18].

It follows that the proposed scheme outperformed the previous schemes significantly for the VIS-NIR and CUHK datasets yielding an average error that is three fold smaller. For the VEDAI dataset, both Aguilera et al. [4] and the proposed scheme achieved a zero error.

## 5 Conclusions

In this work we presented a Deep-Learning-based approach for the matching of image patches in multimodal images, that utilizes a novel Hybrid formulation consisting of two CNN sub-networks. The first is a Siamese (dual weigh-sharing) CNN, while the second is an asymmetric (dual non-weigh-sharing) CNN. We show that the training convergence and test accuracy are improved by applying auxiliary losses to the Siamese and asymmetric sub-networks, alongside the main output loss. We also propose a negative mining scheme adapted for the

<sup>3</sup><https://github.com/ensv/TS-Net>

<sup>4</sup><https://github.com/ngunsu/lcsis>  
<https://github.com/ngunsu/qnet>

<sup>5</sup><https://github.com/ngunsu/LGHD>

Network/descriptor	Field	Forest	Indoor	Mountain	Old building	Street	Urban	Water	Mean
SIFT [18]	39.44	11.39	10.13	28.63	19.69	31.14	10.85	40.33	23.95
LGHD [3]	16.52	3.78	7.91	10.66	7.91	6.55	7.21	12.76	9.16
Siamese [4]	15.79	10.76	11.6	11.15	5.27	7.51	4.6	10.21	9.61
Pseudo Siamese [4]	17.01	9.82	11.17	11.86	6.75	8.25	5.65	12.04	10.32
2Channel [4]	9.96	<b>0.12</b>	4.4	8.89	2.3	<b>2.18</b>	1.58	6.4	4.47
Q-Net 2P-4N [5]	26.03	5	9.46	18.21	7.75	11.16	5.46	17.8	12.60
TS-Net [10]	25.45	31.44	33.96	21.46	22.82	21.09	21.9	21.02	24.89
<b>Hybrid-Softmax</b>	10.12	6.4	9.34	7.82	4.31	5.01	3.11	7.09	6.74
<b>Hybrid-Softmax-HM</b>	5.88	1.45	6.93	3.5	<b>2.25</b>	2.37	<b>0.99</b>	<b>3.06</b>	2.97
<b>Hybrid-<math>L_2</math></b>	19.95	19.49	18.98	18.79	13.99	14.26	14.5	17.46	17.7
<b>Hybrid-<math>L_2</math>- HM</b>	<b>5.65</b>	0.75	<b>3.72</b>	<b>3.99</b>	2.62	2.21	2.04	<b>3.06</b>	<b>2.77</b>

Table 3: Patch matching results evaluated using the VIS-NIR dataset and the patches extracted as in Aguilera et al. [4, 5]. The accuracy is given in terms of the FPR95 score, and the leading results are marked in **bold**. The schemes names in bold are variations of the proposed scheme, and the acronym HM relates to using the proposed hard mining scheme.

patch matching problem. The proposed scheme is experimentally shown to compares favorably with contemporary state-of-the-art approaches when applied to multiple multimodal image datasets.

## References

- [1] S. Agarwal, Y. Furukawa, N. Snavely, I. Simon, B. Curless, S. M. Seitz, and R. Szeliski. Building rome in a day. *Communications of the ACM*, 54(10):105–112, 2011. 1
- [2] C. Aguilera, F. Barrera, F. Lumbreras, A. D. Sappa, and R. Toledo. Multispectral image feature points. *Sensors*, 12(9):12661–12672, 2012. 1, 2, 3
- [3] C. Aguilera, A. D. Sappa, and R. Toledo. Lghd: A feature descriptor for matching across non-linear intensity variations. In *Image Processing (ICIP), 2015 IEEE International Conference on*, page 5. IEEE, Sep 2015. 2, 3, 7, 8, 9
- [4] C. A. Aguilera, F. J. Aguilera, A. D. Sappa, C. Aguilera, and R. Toledo. Learning cross-spectral similarity measures with deep convolutional neural networks. In *The IEEE Conference on Computer Vision and Pattern Recognition (CVPR) Workshops*, page 9. IEEE, Jun 2016. 2, 3, 6, 7, 8, 9
- [5] C. A. Aguilera, A. D. Sappa, C. Aguilera, and R. Toledo. Cross-spectral local descriptors via quadruplet network. *Sensors*, 17(4):873, 2017. 2, 3, 5, 6, 7, 8, 9
- [6] A. Z. Broder. Identifying and filtering near-duplicate documents. In *Proceedings of the 11th Annual Symposium on Combinatorial Pattern Matching*, COM ’00, pages 1–10, Berlin, Heidelberg, 2000. Springer-Verlag. 2, 4, 5
- [7] M. Brown and S. Süssstrunk. Multi-spectral sift for scene category recognition. In *Computer Vision and Pattern Recognition (CVPR), 2011 IEEE Conference on*, pages 177–184. IEEE, 2011. 6
- [8] J. Chen and J. Tian. Real-time multi-modal rigid registration based on a novel symmetric-sift descriptor. *Progress in Natural Science*, 19(5):643–651, 2009. 2, 3
- [9] C. B. Choy, J. Gwak, S. Savarese, and M. Chandraker. Universal correspondence network. In *Advances in Neural Information Processing Systems*, pages 2414–2422, 2016. 5
- [10] S. En, A. Lechervy, and F. Jurie. Ts-net: Combining modality specific and common features for multimodal patch matching. *arXiv preprint arXiv:1806.01550*, 2018. 2, 3, 6, 7, 8, 9
- [11] A. Gionis, P. Indyk, and R. Motwani. Similarity search in high dimensions via hashing. In *Proceedings of the 25th International Conference on Very Large Data Bases, VLDB ’99*, pages 518–529, San Francisco, CA, USA, 1999. Morgan Kaufmann Publishers Inc. 2, 4, 5
- [12] M. Hasan, M. R. Pickering, and X. Jia. Modified sift for multi-modal remote sensing image registration. In *Geoscience and Remote Sensing Symposium (IGARSS), 2012 IEEE International*, pages 2348–2351. IEEE, 2012. 1, 3
- [13] M. T. Hossain, G. Lv, S. W. Teng, G. Lu, and M. Lackmann. Improved symmetric-sift for multi-modal image



Network/descriptor	VEDAI	CUHK	VIS-NIR
SIFT[18]	42.74	5.87	32.53
LGHD[3]	1.31	0.65	10.76
2Channel[4]	<b>0</b>	0.39	11.32
Q-Net 2P-4N[5]	0.78	0.9	22.5
Siamese[10]	0.84	3.38	13.17
Pseudo Siamese[10]	1.37	3.7	15.6
TS-Net[10]	0.45	2.77	11.86
Hybrid-Softmax	0.03	0.23	5.78
Hybrid-Softmax-HM	<b>0</b>	0.05	<b>3.66</b>
Hybrid- $L_2$	<b>0</b>	0.29	9.9
Hybrid- $L_2$ -HM	<b>0</b>	<b>0.1</b>	3.41

Table 4: Patch matching results evaluated using the VIS-NIR, VEDAI and CUHK datasets, where the patches were extracted using a uniform lattice layout [10]. The accuracy is given in terms of the FPR95 score, and the leading results are marked in **bold**. The schemes names in bold are variations of the proposed scheme, and the acronym HM relates to using the proposed hard mining scheme.

- registration. In *Digital Image Computing Techniques and Applications (DICTA)*, 2011 *International Conference on*, pages 197–202. IEEE, 2011. 2, 3
- [14] M. Irani and P. Anandan. Robust multi-sensor image alignment. In *Computer Vision, 1998. Sixth International Conference on*, pages 959–966. IEEE, 1998. 1, 2, 3
- [15] Y. Keller and A. Averbuch. Multisensor image registration via implicit similarity. *IEEE transactions on pattern analysis and machine intelligence*, 28(5):794–801, 2006. 1, 2, 3
- [16] Y. P. Kwon, H. Kim, G. Konjevod, and S. McMains. Dude (duality descriptor): A robust descriptor for disparate images using line segment duality. In *Image Processing (ICIP), 2016 IEEE International Conference on*, pages 310–314. IEEE, 2016. 2, 3
- [17] H. Li, B. Manjunath, and S. K. Mitra. A contour-based approach to multisensor image registration. *IEEE transactions on image processing*, 4(3):320–334, 1995. 1, 2
- [18] D. G. Lowe. Distinctive image features from scale-invariant keypoints. *International journal of computer vision*, 60(2):91–110, 2004. 1, 2, 3, 7, 8, 9
- [19] S. Razakarivony and F. Jurie. Vehicle detection in aerial imagery: A small target detection benchmark. *Journal of Visual Communication and Image Representation*, 34:187–203, 2016. 6, 7
- [20] E. Simo-Serra, E. Trulls, L. Ferraz, I. Kokkinos, P. Fua, and F. Moreno-Noguer. Discriminative learning of deep convolutional feature point descriptors. In *Proceedings of the IEEE International Conference on Computer Vision*, pages 118–126, 2015. 2, 5
- [21] A. Sotiras, C. Davatzikos, and N. Paragios. Deformable medical image registration: A survey. *IEEE transactions on medical imaging*, 32(7):1153–1190, 2013. 1
- [22] C. Szegedy, W. Liu, Y. Jia, P. Sermanet, S. Reed, D. Anguelov, D. Erhan, V. Vanhoucke, and A. Rabinovich. Going deeper with convolutions. In *Proceedings of the IEEE conference on computer vision and pattern recognition*, pages 1–9, 2015. 5
- [23] E. Tola, V. Lepetit, and P. Fua. Daisy: An efficient dense descriptor applied to wide-baseline stereo. *IEEE transactions on pattern analysis and machine intelligence*, 32(5):815–830, 2010. 2
- [24] D. Vaquero, M. Turk, K. Pulli, M. Tico, and N. Gelfand. A survey of image retargeting techniques. In *Proc. SPIE*, volume 7798, page 779814, 2010. 1
- [25] A. Vedaldi and K. Lenc. Matconvnet: Convolutional neural networks for matlab. In *Proceedings of the 23rd ACM international conference on Multimedia*, pages 689–692. ACM, 2015. 6
- [26] P. Viola and W. M. Wells, III. Alignment by maximization of mutual information. *Int. J. Comput. Vision*, 24(2):137–154, Sept. 1997. 1, 3
- [27] X. Wang and X. Tang. Face photo-sketch synthesis and recognition. *IEEE Transactions on Pattern Analysis and Machine Intelligence*, 31(11):1955–1967, 2009. 6, 7
- [28] S. Zagoruyko and N. Komodakis. Learning to compare image patches via convolutional neural networks. In *Proceedings of the IEEE Conference on Computer Vision and Pattern Recognition*, pages 4353–4361, 2015. 2, 3
- [29] B. Zitova and J. Flusser. Image registration methods: a survey. *Image and vision computing*, 21(11):977–1000, 2003. 1

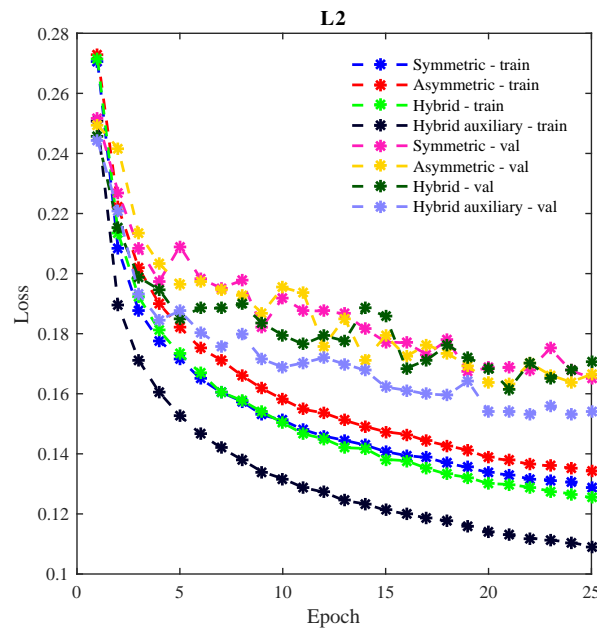
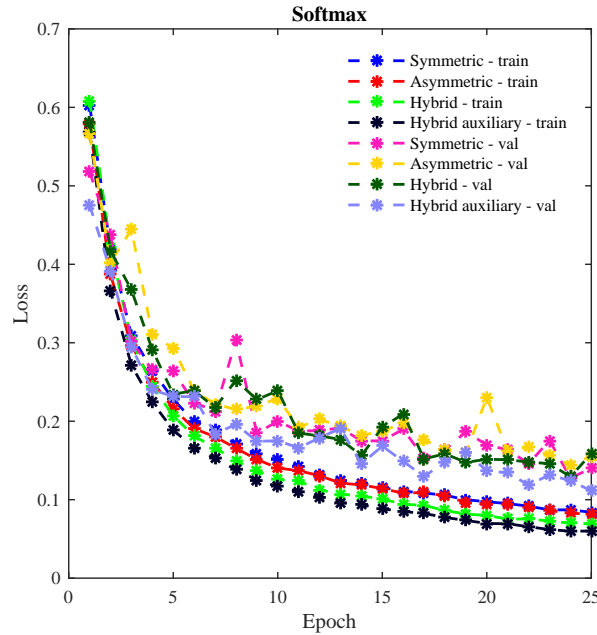


Figure 5: The training and validation losses for different patch matching CNN architectures: symmetric (Siamese), asymmetric, Hybrid and hybrid with auxiliary losses CNNs. The Softmax and  $L_2$  losses are shown in (a) and (b), respectively.

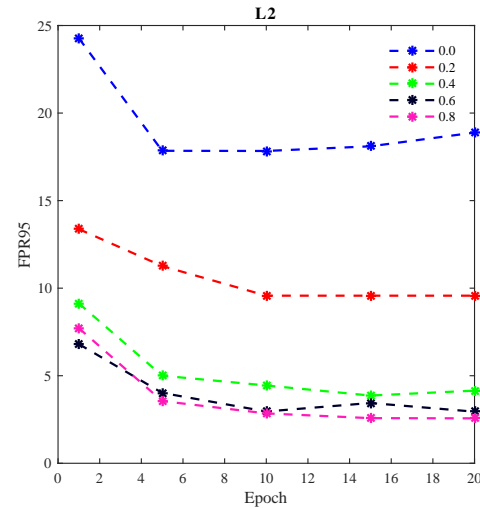
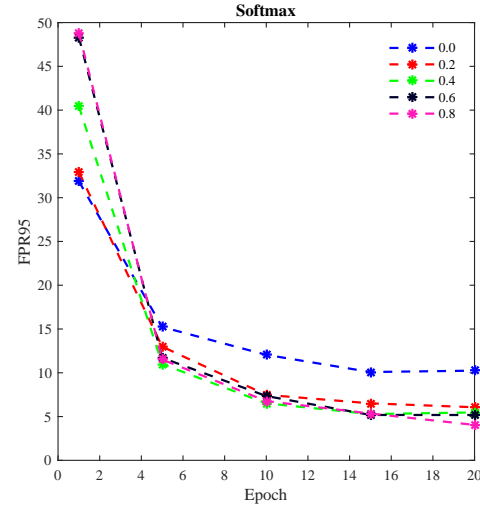


Figure 6: Classification accuracy of the validation set in terms of the FPR95 score, for different values of the hard negative mining measure  $h_m$ . As  $h_m \rightarrow 1$  the number of negative pairs increases. The results of training using the Softmax and  $L_2$  losses are shown in (a) and (b), respectively.